A Convoy Protection Strategy Using the Moving Path Following Method

Tiago Oliveira[1], A. Pedro Aguiar[2] and Pedro Encarnação[3]

***Abstract*— This paper considers the problem of convoy protection missions using a fixed-wing Unmanned Aerial Vehicle (UAV) in scenarios where the radius of the circular region of interest around the convoy is smaller than the UAV minimum turning radius. Using the Moving Path Following (MPF) method, we propose a guidance algorithmic strategy where a UAV moving at constant ground speed is required to converge to and follow a desired geometric moving path that is attached to the convoy center. Conditions under which the proposed strategy solves the convoy problem are derived. A performance metric that is proposed together with numerical simulation results demonstrate the effectiveness of the proposed approach.**

I. Introduction

Target tracking and convoy protection missions using Unmanned Aerial Vehicles (UAV) are an active area of research for both civilian and military applications. In order to perform such tasks, the UAVs are typically equipped with electro-optical sensors with a given resolution and thus, the most suitable trajectory for the UAV depends (among other things) on the required level of image resolution. Considering the case where the mission is performed during long periods of time or if it is expected that the UAV travels long distances, then a fixed-wing UAV is typically employed.

The work described in [1] addresses the problem of controlling a group of UAVs to provide convoy protection to a group of ground vehicles, where the radius of the circular region of interested (which is determined by the optical sensor's resolution carried by the UAVs) is smaller than the UAVs minimum turning radius. For the case of a single UAV and when the ground convoy of vehicles is restricted to be stationary or moving in straight lines at constant speed, the authors analyse what is the best UAV path in the sense that it maximizes the longest time that the UAV is inside the convoy circular region of interest, and provide a lower bound on the convoy speed (that depends on the ratio between the radius of the convoy circular region of interest and the UAV minimum turning radius) that guarantees continuous convoy protection at all times (i.e., the UAV will always be inside the convoy circular region of interest, despite the UAV's kinematic constraints that are modeled as Dubins vehicles). Notice, however, that these results only apply for a very particular restricted convoy trajectory case. For a more general target tracking/convoy protection missions, the typical adopted strategy reported in the literature is to make the fixed-wing UAV to be at a given standoff distance from the target/convoy center [2], [3], [4], [5]. In alternative, in [6], [7], lateral and longitudinal orbits (depending on the convoy speed) are proposed in order to perform convoy protection missions. The method chooses the most adequate desired path depending on the speed ratio between the UAV and the convoy. However, none of these strategies encompass the case presented in [1] where the radius of the convoy circular region of interest is smaller than the UAV minimum turning radius, and often do not take into account the UAV's kinematic constraints [2], [5]. In this paper we consider the problem of convoy protection guaranteeing a continuous time coverage and without the restrictions on the convoy movements presented in [1].

We make use of the MPF method to solve this problem, where a fixed-wing UAV moving at constant ground speed is required to converge to and follow a desired geometric path that is attached to the target/convoy center [8], [9]. The MPF method can be applied to the general case of desired paths moving with respect to an inertial coordinate frame with time-varying linear and angular velocities, and with non-constant curvature, thus generalizing the classical path following that only deals with stationary paths. MPF methods, by design, retain the desirable characteristics of the classical path following method, namely smooth convergence to the moving path and the possibility of doing so at constant speed with respect to an inertial coordinate frame [9]. By explicitly taking into account UAV's physical constraints, this paper formally addresses the necessary conditions for the moving path's geometry, linear and angular velocities with respect to the inertial frame that must be verified in order to ensure that the MPF problem is well posed. Particularly, our proposed strategy is to attach the desired path to the convoy center and command the desired path's angular velocity such that the UAV's resulting trajectory complies with the UAV's physical constraints.

We emphasize that the MPF method is not limited to a standoff circle centered at the target/convoy center position (unlike most of the proposed methods in the literature [2], [3], [5]) and allows the use of any geometric path shape (satisfying the UAV's physical constraints) attached to the desired target. A discussion on the desired path's best suited geometric shape for the proposed problem is also included. Illustration and validation of the proposed strategy is provided through numerical simulations, convergence guaran-

[1]T. Oliveira is with the Portuguese Air Force Academy Research Center, Sintra, 2715-021, Portugal. tmoliveira@academiafa.edu.pt

[2]A. P. Aguiar is with the Research Center for Systems and Technologies (SYSTEC), Faculty of Engineering of the University of Porto (FEUP), and Institute for Systems and Robotics (ISR), Portugal. pedro.aguiar@fe.up.pt

[3]P. Encarnação is with the UCP - Católica Lisbon School of Business & Economics, Lisbon, Portugal. pme@ucp.pt

This work was partially supported by project POCI-01-0145-FEDER-006933/SYSTEC funded by FEDER funds through COMPETE2020 and by national funds through the Fundação para a Ciência e a Tecnologia (FCT).

tees and performance metrics.

The paper is organized as follows. Section II presents the convoy protection problem formulation. Then, Section III introduces briefly the MPF problem formulation and its error space. Section IV presents the MPF method as a solution for the convoy protection problem. Numerical simulation results and performance metrics are included in Section V. Finally, Section VI contains the main conclusions and future work.

II. Convoy protection problem formulation

Consider a local inertial frame $\{I\} = \{\overrightarrow{x}, \overrightarrow{y}\}$ with the $\overrightarrow{x}$ axis pointing North and $\overrightarrow{y}$ East. Let ψ be the angle between the vehicle velocity vector and North (we assume that the UAV is flying at constant altitude). Additionally, let V be the UAV ground speed. The UAV kinematic equations expressed in $\{I\}$ are given by

$$\begin{aligned} \dot{x} &= V\ \cos\psi \\ \dot{y} &= V\ \sin\psi. \\ \dot{\psi} &= \omega \qquad \text{with } \omega \in [-\omega_{max}, \omega_{max}] \end{aligned} \tag{1}$$

where ω_{max} represents the bound on the yaw rate, and $r_{min} = \frac{V}{\omega_{max}}$ is the minimum turning radius of the UAV.

In this paper, we assume that the cameras on board the UAV can monitor a disk of radius r_c on the ground irrespectively of the UAV attitude, i.e., we assume that the on board camera is attached to a gimballed structure and is always looking down, independently of the attitude of the UAV. For convenience, ground convoys are considered to be a point located at the centroid of the convoys in the $\overrightarrow{x} - \overrightarrow{y}$ plane. Similar to [1], we consider that a successful convoy protection is being achieved when the centroid of the convoy is visible to the UAV at any time, i.e., if the distance between the projection of the UAV onto the $\overrightarrow{x} - \overrightarrow{y}$ plane and the centroid of the convoy is less than or equal to r_c (see Figure 1).

Typically, in order to ensure a high level of image resolution, the on board sensors may have a narrow field of view which, depending on the flight altitude, may impose an observation disk radius r_c smaller than the minimum turning radius of the UAV r_{min}.

In this case, where $r_{min} > r_c$, depending on the convoy trajectory and speed relative to the UAV, it might be possible to fly out of this circle, and therefore not be able to guarantee continuous convoy protection.

The problem addressed in this paper can be formalized as: Consider a convoy that is arbitrarily moving with possible time-varying linear and angular velocities and a single fixed-wing UAV with a kinematic constrained model given by equations (1). Derive a guidance algorithm that sets the UAV speed V and angular velocity ω such that the time that the convoy center remains within the UAV sensor footprint (that is assumed to be smaller than the UAV minimum turning radius) is maximized. Furthermore, provide conditions under which the proposed scheme guarantees continuous convoy protection (i.e., the UAV will always be inside the convoy circular region of interest).

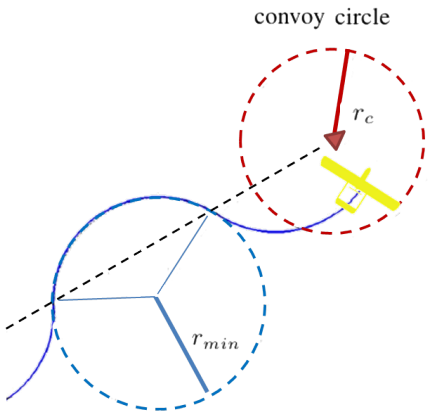

Fig. 1. Convoy protection problem formulation illustration. The convoy center is represented by the red triangle. Adapted from [1]. We consider the case where the minimum turning radius of the UAV (r_{min}) is greater than r_c.

III. Moving path following problem formulation

This section reviews the MPF problem and derives the corresponding kinematic error space with respect to the Serret-Frenet frame [10], [11] associated to a given reference planar path. Full details about the MPF error space derivation can be found in [9]. A MPF control law will be used in Section IV to address the problem formulated in Section II.

A. MPF error space

Consider a path-transport frame $\{P\} = \{\overrightarrow{x}_P, \overrightarrow{y}_P\}$ and let the origin of $\{P\}$ expressed in $\{I\}$ be denoted by p_0. Let ${}^P p_d(\ell)$ be a desired planar geometric path parametrized by ℓ, which for convenience will be assumed to be the path length. Note that given a fixed $\ell \geq 0$, ${}^P p_d(\ell)$ is a point on the path expressed in the path-transport frame. Additionally, let $v_d = \dot{p}_0 = \begin{bmatrix} v_{d_x} & v_{d_y} \end{bmatrix}^T$ and ω_d be the corresponding linear and angular velocities of the path-transport frame $\{P\}$, respectively, expressed in $\{I\}$. In practice, the path-transport frame specifies the desired motion of the path with respect to the inertial frame and a desired geometric path is considered to be a moving path whenever v_d or ω_d are different from zero.

The MPF problem can thus be formulated as follows: Given a robotic vehicle moving at a given speed V and a desired moving path $\mathcal{P}_d = \left({}^P p_d(\ell), p_0, v_d, \omega_d\right)$, design a control law that steers and keeps the vehicle on the desired path $\mathcal{P}_d$.

Let $\{F\} = \{\overrightarrow{t}, \overrightarrow{n}\}$ be the Serret-Frenet frame associated to the desired path and $\kappa(\ell)$ the path curvature. Additionally, a wind frame $\{W\} = \{\overrightarrow{x}_W, \overrightarrow{y}_W\}$ is considered, located at the vehicle's center of mass, with its $\overrightarrow{x}_W$-axis along the direction of the vehicle velocity vector and $\overrightarrow{y}_W$ pointing to the right of an observer looking along $\overrightarrow{x}_W$ (see Figure 2).

The vehicle center of mass coordinates are denoted by $p_F = \begin{bmatrix} x_F & y_F \end{bmatrix}^T$ when expressed in the Serret-Frenet frame. Setting the origin of $\{F\}$ at the path point p_d that is the closest to the vehicle, it follows that $p_F = \begin{bmatrix} 0 & y_F \end{bmatrix}^T$.

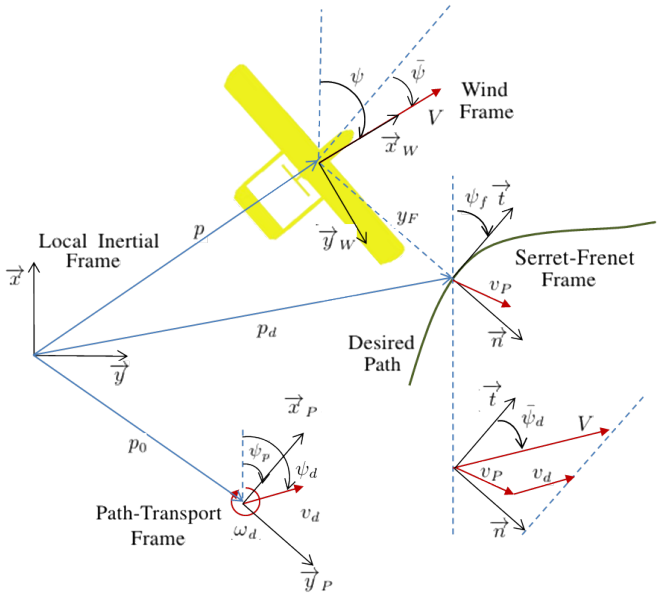

Fig. 2. Moving path following: Error space frames and relevant variables, illustrating the case of a UAV. Adopted from [9].

Furthermore, let $(p_d - p_0) = \begin{bmatrix} \Delta x & \Delta y \end{bmatrix}^T$ be the vector from the origin of $\{P\}$ to the origin of $\{F\}$.

Finally, let ψ_p be the angle that parametrizes the rotation matrix from $\{I\}$ to $\{P\}$ (thus, by definition $\omega_d = \dot{\psi}_p$), let ψ_d be the angle between the linear velocity v_d and the $\vec{x}$ axis, and let ψ be the angle between the vehicle velocity vector and the North direction. Additionally, let ψ_f be the yaw angle that parametrizes the rotation matrix from $\{I\}$ to $\{F\}$. The angular displacement between the wind frame and the Serret-Frenet frame is $\bar{\psi} = \psi - \psi_f$ (see Figure 2).

Considering the above notation, the error kinematic model for MPF is given by [9]

$$\begin{aligned} \dot{\ell} &= \frac{V\cos\bar{\psi} - (v_{d_x} - \omega_d\,\Delta y)\cos\psi_f}{1-\kappa(\ell)\,y_F} \\ &\quad - \frac{\left(v_{d_y} + \omega_d\,\Delta x\right)\sin\psi_f - \omega_d\,y_F}{1-\kappa(\ell)\,y_F} \\ \dot{y}_F &= V\sin\bar{\psi} + (v_{d_x} - \omega_d\,\Delta y)\sin\psi_f - \left(v_{d_y} + \omega_d\,\Delta x\right)\cos\psi_f \\ \dot{\bar{\psi}} &= \dot{\psi} - \kappa(\ell)\,\dot{\ell} - \omega_d, \end{aligned} \tag{2}$$

where it is assumed that $1-\kappa(\ell)\,y_F \neq 0$, which corresponds to the vehicle not being exactly at the distance from the path point p_d (the closest path point to the vehicle - parametrized by ℓ) that corresponds to the inverse of the path's curvature at that point. This singularity could be avoided using a "virtual target" to specify the desired position of the UAV on the path, not necessarily coincident with the projection of the vehicle on the path (and thus x_F wouldn't necessarily be zero). By choosing the speed of the virtual target along the path it is possible to remove the singularity. Further details of this method can be found in [12], [13]. In this paper we assume that $1 - \kappa(\ell)\,y_F \neq 0$ and that the vehicle speed V is constant. The method in [12], [13] can be used on top of the control law derived here to ensure that the UAV never crosses the singularity.

The MPF error space in (2) will be used in the sequel to derive the desired path's linear and angular velocities v_d and ω_d in order to solve the problem formulated in Section II.

B. MPF kinematic constraints

Considering the kinematic model (2), the steady state value $\bar{\psi}_d$ for ψ can be computed by setting $\dot{y}_F = 0$, which yields

$$\bar{\psi}_d = \arcsin\left(\frac{-\left(v_{d_x} - \omega_d\,\Delta y\right)\sin\psi_f + \left(v_{d_y} + \omega_d\,\Delta x\right)\cos\psi_f}{V}\right) \tag{3}$$

In order to ensure that equation (3) is always well defined, one may have to introduce some restrictions on the chosen path's geometry or *dynamics* since it depends on the relation between the path's linear and angular velocities and also on the displacement between the origin of the path-transport frame and the Serret-Frenet frame $(\Delta x, \Delta y)$. More specifically, by setting the absolute value of the argument of the arc of sine in (3) less than 1 and solving for ω_d one gets

$$|\omega_d| < \frac{V - v_d\,\sin\left(\psi_d - \psi_f\right)}{\sqrt{\Delta x^2 + \Delta y^2}\,\left|\sin\left(\psi_f + \arctan\left(\frac{\Delta y}{\Delta x}\right)\right)\right|} \quad \text{and}$$
$$v_d < V. \tag{4}$$

A MPF control law should drive the lateral distance y_F and heading error $\tilde{\psi} = \bar{\psi} - \bar{\psi}_d$ to zero. Thus, from equation (2), the steady state value for $\dot{\psi}$ (where $\dot{\tilde{\psi}} = 0$) will be

$$\dot{\psi} = \dot{\bar{\psi}}_d + \kappa(\ell)\,\dot{\ell} + \omega_d. \tag{5}$$

In order to take into account the vehicle kinematic constraints $|\omega| < \omega_{max}$ (see equation (1)), it is now straightforward to conclude that condition

$$|\dot{\bar{\psi}}_d + \kappa(\ell)\,\dot{\ell} + \omega_d| \leq \omega_{max} \tag{6}$$

must also be ensured for the MPF problem to be always well posed. Notice that $\dot{\bar{\psi}}_d$ and $\dot{\ell}$ also depend on the variables v_d and ω_d. Thus, intuitively, it is possible to command the desired path linear and angular velocities (v_d and ω_d) to ensure that the condition (6) always holds and thus the MPF problem is well posed, for any given path's curvature $\kappa(\ell)$. In other words, it is *in principle* possible to make the UAV follow a given desired path geometry (with a given path curvature $\kappa(\ell)$) that wouldn't be possible using the classical path following methods (where $v_d = \omega_d = 0$). This degree of freedom will be explored in Section IV such that the path movement is chosen to ensure that a UAV running the MPF control law [9]

$$\begin{aligned} \dot{\psi} = &-g_1\,\tilde{\psi} + \kappa\,(\ell)\;\dot{\ell} + \omega_d + \dot{\bar{\psi}}_d \\ &- g_2\,y_F(((v_{d_x} - \omega_d\,\Delta y)\,\sin\psi_f \\ &- \left(v_{d_y} + \omega_d\,\Delta x\right)\,\cos\psi_f)\,\frac{1-\cos\tilde{\psi}}{\tilde{\psi}} \\ &+ V\,\cos\bar{\psi}_d\frac{\sin\tilde{\psi}}{\tilde{\psi}}) \end{aligned} \tag{7}$$

converges to that path, thus providing convoy protection. Parameters g_1 and g_2 are positive scalars assigning relative weights between position and orientation errors.

IV. Convoy Protection using MPF

In this section we propose a MPF method to solve the problem formulated in Section II.

A. Proposed strategy

Consider a lemniscate path that is contained within a circle of radius r_c as shown in Figure 3. Our proposed strategy is to make the UAV follow a moving lemniscate path centered at the target/centroid of convoy position p_t (thus, by definition $p_0 = p_t$, $v_d = v_t$ and $\psi_t = \psi_d$), where v_t and ψ_t are the target/centroid of convoy velocity and heading respectively. Notice however that by imposing this condition on v_d, the path's angular velocity ω_d is still "free" to be chosen and may be used as a control input.

Under the same assumptions considered in [1], first consider that the target moves at a given constant velocity v_d (thus $\dot{v}_d = 0$) and constant heading (thus $\dot{\psi}_d = 0$). Moreover, in order to provide further insight to the proposed method (that is to command the desired path's angular velocity) let us first consider the case in which the path's angular velocity is set to zero ($\dot{\psi}_p = \omega_d = 0$). Intuitively, as in the case considered in [1], the UAV, due to its kinematic constraints, will not be able to follow the desired lemniscate path unless a given lower bound on the target speed is observed, which can be computed as follows.

Considering the above assumptions, condition (6) can be rewritten as

$$\left| \kappa(u)\, \dot{\ell} \left(1 - \frac{v_d \cos\left(\psi_d - \psi_f\right)}{V \sqrt{1 - \left(\frac{v_d \sin(\psi_d - \psi_f)}{V} \right)}} \right) \right| \leq \omega_{max}$$

$$\Leftrightarrow \left| \frac{r_c}{V} \right| \left| \kappa(u)\, \dot{\ell} \left(1 - \frac{v_d \cos\left(\psi_d - \psi_f\right)}{V \sqrt{1 - \left(\frac{v_d \sin(\psi_d - \psi_f)}{V} \right)}} \right) \right| \leq \frac{r_c}{r_{min}} \tag{8}$$

where (see equation (2))

$$\dot{\ell} = V \left(\sqrt{1 - \left(\left(\frac{v_d}{V} \right)^2 \sin^2\left(\psi_d - \psi_f\right) \right)} - \frac{v_d \cos\left(\psi_d - \psi_f\right)}{V} \right),$$

and the desired lemniscate path curvature κ and tangential angle ψ_f are [14]

$$\kappa\left(u\right) = \frac{-3\sqrt{2}\, \cos\left(\langle u \rangle\right)}{r_c \sqrt{3 - 2\cos\left(2\, \langle u \rangle\right)}}, \tag{9}$$

$$\psi_f\left(\psi_p, u\right) = 3\, \arctan\left(\sin\left(\langle u \rangle\right)\right) + \psi_p, \tag{10}$$

with $\langle u \rangle \triangleq u \mod 2\pi$ and mod is the modulus operator that makes $u \in [0\ \ 2\pi]$. The parameter u is related to the path length ℓ through $\ell(u) = \sqrt{2}\, r_c \int_0^u \left[3 - \cos(2\, u)\right]^{-\frac{1}{2}}\, du$ [14]. Note that from the above definition, a given fixed u parametrizes a point on the desired path expressed in the path-transport frame.

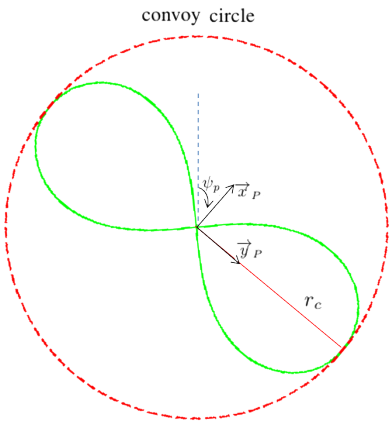

Fig. 3. Convoy protection using the MPF method: relevant variables.

Let the left-hand side of equation (8) be designated by $f\left(\frac{v_d}{V}, u, \psi_p\right)$. From the problem formulation presented in Section II, one must ensure that $f\left(\frac{v_d}{V}, u, \psi_p\right) \leqslant 1$. A first observation is that the maximum of $f\left(\frac{v_d}{V}, u, \psi_p\right)$ is independent of ψ_d, which means that the target can move in a straight line in any direction ψ_d without introducing any additional constraint to the problem.

An analytic solution of equation (8) with respect to $\frac{v_d}{V}$ (in order to compute the lower bound on the target speed) can not be derived. Figure 4 illustrates $f\left(0.5, u, \psi_p\right)$ and $f\left(1, u, \psi_p\right)$ for $u \in \left[\ 0,\quad 2\,\pi\ \right]$, $\psi_p \in \left[\ -\frac{\pi}{2},\quad \frac{\pi}{2}\ \right]$ and $\frac{v_d}{V}$ equal to 0.5 and 1 respectively. It is assumed, without loss of generality (for the case of a target moving in straight line), that $\psi_d = 0$. This leads to the following conclusions:

1) for a constant ψ_p (which follows from the fact that ω_d is set to zero), the UAV will increase u at all the times (because from the path following definition one has $\dot{u} > 0$) and thus one obtains $f\left(\frac{v_d}{V}, u, \psi_p\right) \geqslant 1$ for every constant $\psi_p \in \left[-\frac{\pi}{2},\quad \frac{\pi}{2}\right]$, as it can be seen from Figure 4. Therefore, it is not possible for the UAV to follow the desired lemniscate path contained within the circle r_c keeping the desired path's angular velocity $\dot{\psi}_p = \omega_d$ always equal to zero, even for the case where $\frac{v_d}{V} \approx 1$ [1];
2) there exists a lower bound on $\frac{v_d}{V}$ from which $\exists\left(u, \psi_p\right)$, with $u \in \left[\ 0,\quad 2\,\pi\ \right]$ and $\psi_p \in \left[\ -\frac{\pi}{2},\quad \frac{\pi}{2}\ \right]$: $f\left(\frac{v_d}{V}, u, \psi_p\right) \leqslant 1$. Thus, for every path point parametrized by u, it is possible to compute a desired path orientation ψ_p as a function of u, such that from a given lower bound on the $\frac{v_d}{V}$ ratio, $\psi_p\left(u\right) \rightarrow f\left(\frac{v_d}{V}, u, \psi_p\left(u\right)\right) \leqslant 1$. In practice, one should use the degree of freedom of the path's orientation ψ_p by controlling the angular velocity $\dot{\psi}_p = \omega_d$ (subject to the condition (6)) in order to make the UAV to be able

[1] Note that for the case where $\frac{v_d}{V} = 1$, one obtains $\dot{\ell} = 0$ and thus the UAV would follow a given fixed path point and move in a straight line parallel to the target (see also Figure 5 and its description).

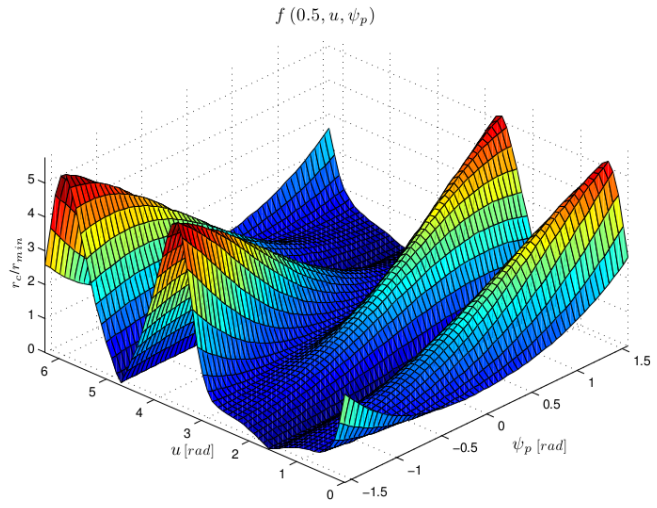

(a)

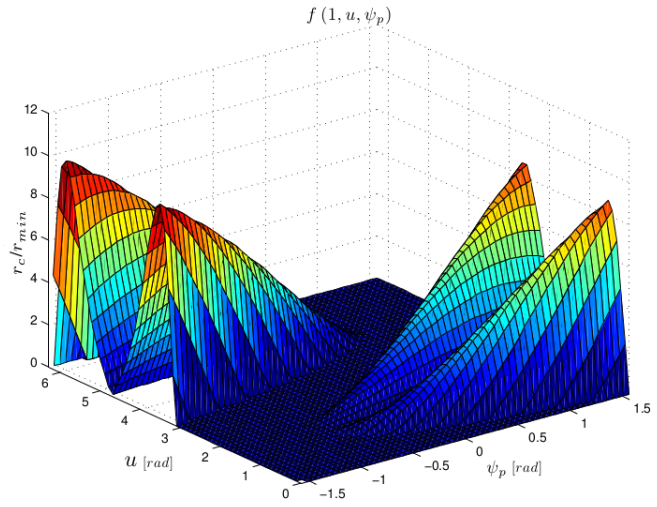

(b)

Fig. 4. Minimum feasible turning radius r_c/r_{min} for a UAV to follow a lemniscate path contained within a circle of radius r_c, considering a): $\frac{v_d}{V} = 0.5$ and b): $\frac{v_d}{V} = 1$.

to follow the moving geometric path.

Figure 5 provides further intuition to the above conclusions. It presents a simulation example where a UAV follows a moving lemniscate path centered at the target/convoy center that is initially located at the inertial frame origin and starts moving with constant heading and velocity ($\psi_d = 0$ and $\frac{v_d}{V} = 0.9$ respectively) towards North. The desired geometric path orientation is kept constant ($\dot{\psi}_p = \psi_p = 0$) and no kinematic constraints for the UAV were imposed. For a long period of time (due to the high ratio $\frac{v_d}{V}$) the UAV flies almost parallel to the target. However, at a given path point, the corresponding path curvature makes the UAV to change its bank angle at a very high rate, making it impossible to comply with its actual kinematic constraints. If one could control the path's angular velocity ω_d, it would be possible to smooth the obtained trajectory (considering the same geometric path and $\frac{v_d}{V}$ ratio) in order to comply with

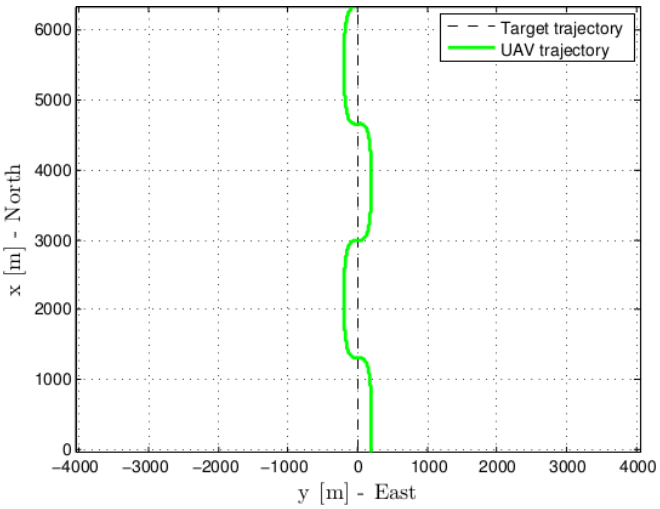

Fig. 5. UAV trajectory following a moving lemniscate path with $\frac{v_d}{V} = 0.9$, $\psi_d = 0$ and $\psi_p = 0$ without imposing any kinematic constraint on the UAV.

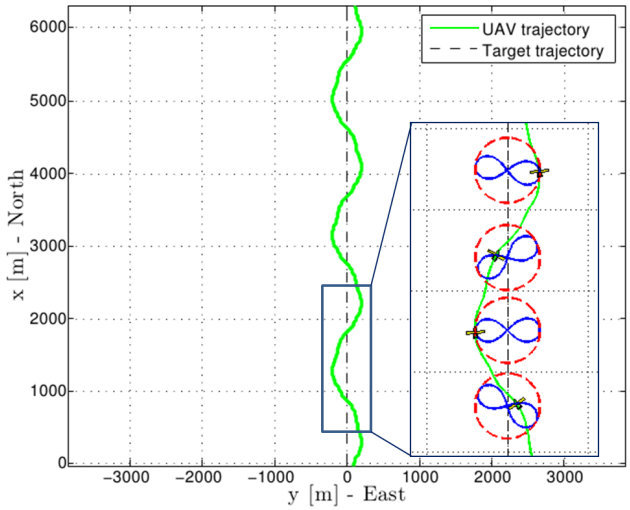

Fig. 6. UAV trajectory following a moving lemniscate path with $\frac{v_d}{V} = 0.9$, $\psi_d = 0$ using Algorithm 1 to control the desired geometric path angular velocity $\dot{\psi}_p = \omega_d$ and orientation angle ψ_p. The obtained trajectory complies with the UAV kinematic constraints.

condition (6) for all path points parametrized by ℓ. This is exactly the idea proposed in this paper. Algorithm 1 describes how it can be implemented.

Figure 6 shows a numerical simulation result considering the same example scenario illustrated in Figure 5 (where a UAV follows a moving lemniscate path centered at the target position with $\frac{v_d}{V} = 0.9$ and $\psi_d = 0$) using Algorithm 1 to control the desired geometric path angular velocity $\dot{\psi}_p = \omega_d$ and orientation angle ψ_p. The convoy circle is depicted in red (with a radius r_c that is equal to the UAV minimum turning radius r_{min}) and the desired geometric path (at given sample time instants) is depicted in blue. The resulting UAV's trajectory (depicted in green) complies with its kinematic constraints and the UAV always remains inside

ALGORITHM 1: Returns the desired geometric path's kinematics.

Input: Vehicle start pose (p, ψ) and velocity V; target's initial position p_0, velocity v_t and heading ψ_t; desired geometric path parameters $\kappa(\ell)$ and $\psi_f(\psi_p.\ell)$; vehicle and convoy circle constraints r_{min} and r_c respectively.

Output: Desired path orientation ψ_p, angular velocity ω_d and angular acceleration $\dot{\omega}_d$.

Initialization:

1. Set $\dot{\omega}_d = \omega_d = 0$;
2. Compute the line of sight angle ψ_{LOS} between the line that connects the target center of mass p_0 to the UAV center of mass p and target's heading direction ψ_d.
3. Set path's initial orientation:

if $\psi_{LOS} \in$ 1st or 3rd quadrant
$\psi_p \leftarrow \psi_d + \frac{\pi}{6}$;
else
$\psi_p \leftarrow \psi_d - \frac{\pi}{6}$;
end

while *target tracking mission is engaged* **do**

4. Compute the path parameter ℓ corresponding to the closest to the UAV point of the path, given UAV's current position p and path's orientation angle ψ_p;
5. Set equations (2) and (3) as a function of ω_d;
6. $\omega_{limit} \leftarrow argmax\{\dot{\ell}(\omega_d)\}$ subject to conditions (4) and (6) and $\dot{\ell}(\omega_d) \geqslant 0 \Rightarrow$ Compute path's desired angular velocity bound that complies with the UAV kinematic constraints;
7. **if** isempty(ω_{limit})

$$\omega_{limit} \leftarrow \frac{V - v_d \sin(\psi_d - \psi_f)}{\sqrt{\Delta x^2 + \Delta y^2}\,|\sin(\psi_f + \arctan(\frac{\Delta y}{\Delta x}))|}$$

end
8. Compute ω_d using a proportional control law:
if $u \in \left[\ \pi \quad 2\pi\ \right]$
$\omega_d \leftarrow k_p\left(\psi_d + \frac{\pi}{6} - \psi_p\right)$ subject to $|\omega_d| \leqslant |\omega_{limit}|$;
else
$\omega_d \leftarrow k_p\left(\psi_d - \frac{\pi}{6} - \psi_p\right)$ subject to $|\omega_d| \leqslant |\omega_{limit}|$;
end
9. $\dot{\omega}_d \leftarrow \frac{d\omega_d}{dt} \Rightarrow$ Compute path's angular acceleration;
10. $\psi_p \leftarrow \int \omega_d \Rightarrow$ Compute path's orientation ψ_p;
11. Update $p \Rightarrow$ Update UAV's current position using the MPF control law given by equation (7) and the UAV kinematic equations (1);
12. Return to 4.

end

the convoy circle[2].

B. Desired path's geometry: lemniscate versus circular path

Under the same assumptions presented in Section IV-A (i.e., target moving with constant heading and speed) consider now the use of a circular path (where by definition $\kappa(u) = \frac{1}{r_c}$ and $\psi_f(\psi_p, u) = u + \psi_p + \frac{\pi}{2}$) for the proposed strategy. Figure 7 shows the minimum feasible turning radius $r_c/r_{min} = f\left(\frac{v_d}{V}, u, \psi_p\right)$ for a UAV to follow a circular path centered at the target position, where $\frac{v_d}{V} = 0.5$ and $\frac{v_d}{V} = 1$. Notice that, starting at a given path point (parametrized by

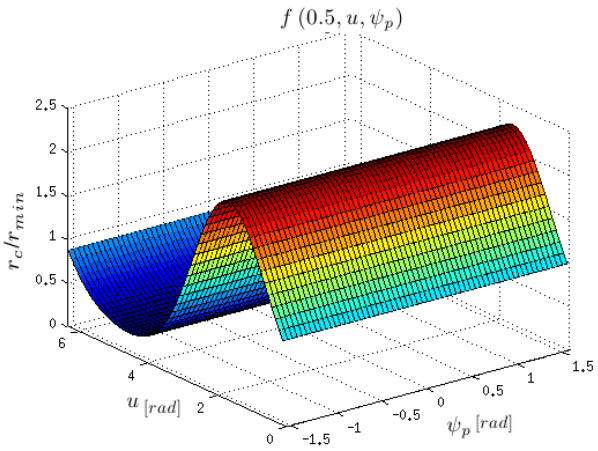

(a)

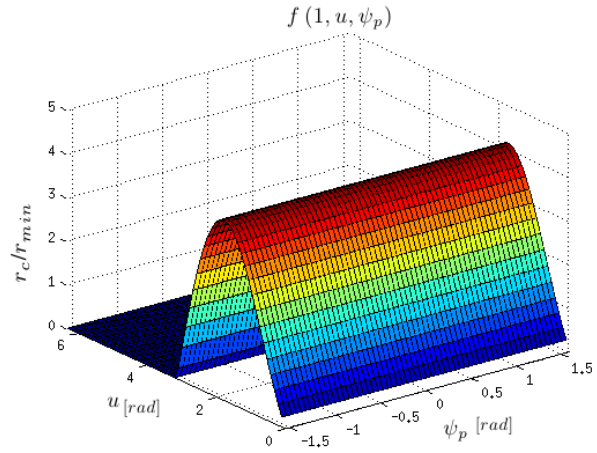

(b)

Fig. 7. Minimum feasible turning radius r_c/r_{min} for a UAV to follow a circular path considering a): $\frac{v_d}{V} = 0.5$ and b): $\frac{v_d}{V} = 1$.

$u \in \left[\ 0, \quad 2\pi\ \right]$), one will always obtain $f\left(\frac{v_d}{V}, u, \psi_p\right) \geqslant 1$ at a given path point, for every constant $\psi_p \in \left[\ -\frac{\pi}{2}, \quad \frac{\pi}{2}\ \right]$. However, unlike the lemniscate path case, it is not possible to control the desired path's orientation [3] $\psi_p(u)$ as a function of u in order to ensure that $f\left(\frac{v_d}{V}, u, \psi_p(u)\right) \leqslant 1$. Thus, one can conclude that, given the considered kinematic constraints, the circular path is not suitable to be used as a solution to the here proposed problem.

The use of a lemniscate path has the following desirable features. First, it allows the UAV to fly over the target/convoy center position periodically, depending on the target's dynamics and the desired path commanded velocity ω_d. Additionally, a lemniscate has been shown to be an effective way for an autonomous aircraft to provide surveillance of a slower target [6], [7]. Despite some of the previously mentioned methods propose a change on the desired path width depending on the target and UAV speed ratio [6]

[2]An illustration video for this simulation can be found in https://www.youtube.com/watch?v=K7dkK6MwmAY

[3]Note that the path orientation for the case of a circular path is, in practice, independent of ψ_p.

or the UAV's kinematic constraints [7], by controlling the lemniscate orientation angle ψ_p (see Figure 3) our solution allows the UAV to stay closer to the target/convoy center, considering the same UAV turn rate constraints (see Figures 5 and 6). Controlling the desired path's orientation instead of its width also ensures smoother trajectories of the UAV when a change on the target's velocity and/or heading occurs. Additionally our proposed solution is, to the authors' best knowledge, the only that encompasses the problem where the UAV minimum turning radius is larger than the radius of the convoy circular region of interest and explicitly takes into account the UAV kinematic constraints. Furthermore, notice that the desired path's angular velocity ω_d is computed in order to maximize the relative velocity of the UAV with respect to the desired path (given by $\dot{\ell}$ - see step 6 of Algorithm 1), which in practice minimizes the time between each pass above the target's position. Finally, note that in the case of a circular path centered at the target position (which is the most common approach in the literature [5]) the UAV's velocity vector (at a given path point) will be pointing exactly in the opposite direction of the target/convoy center velocity vector. The use of a lemniscate path and Step 8 in Algorithm 1 ensures that this situation never occurs which, in practice, translates into less kinematic constraints due to the desired path's geometry.

The best suited path for the proposed problem is still an open issue. Nonetheless, the presented problem formulation simplifies this task, since a given path geometry to be studied (with a given curvature $\kappa(u)$ and tangential angle $\psi_f(\psi_p, u)$) can immediately be used by replacing equations (9) and (10) by those corresponding to the desired path geometry.

The performance results obtained using a lemniscate path are presented in the next section.

V. Numerical results

Three main results for the proposed convoy protection algorithm are presented in this section. First, a lower bound on the convoy/target velocity ratio with respect to the UAV ground speed $\frac{v_d}{V}$ as a function of the ratio between the convoy circle radius and the UAV minimum turning radius $\frac{r_c}{r_{min}}$ is compared with the one presented in [1] under the same assumption that the target moves with constant heading and velocity. Then, we show how these restrictions on the convoy movements can be relaxed using the proposed method through a simulation example that includes time varying linear and angular target velocities. Finally, a performance metric is proposed, considering the case where no lower bound on the target speed is imposed.

A. Lower bound on target velocity

Consider a convoy moving with constant heading and velocity. As in the case considered in [1], due to the UAV kinematic constraints, the UAV will not be able to follow the desired lemniscate path within the convoy circle (given that $r_c < r_{min}$) unless a given lower bound on the target/convoy speed relative to the UAV (expressed by the $\frac{v_d}{V}$ ratio) is achieved.

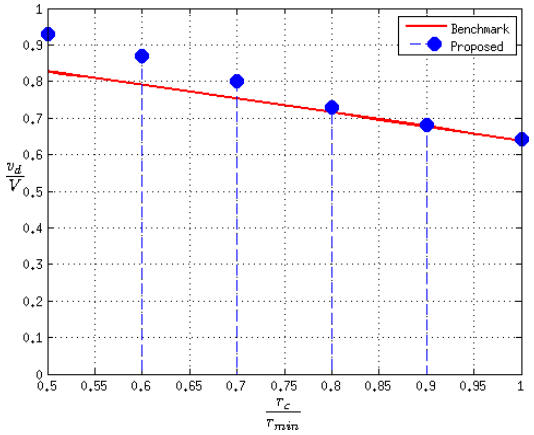

Fig. 8. Lower bound for $\frac{v_d}{V}$ as a function of $\frac{r_c}{r_{min}}$ for the proposed method and the considered benchmark [1].

Due to the complexity of the above derived equations, an analytic solution for equation (8) providing the lower bound for $\frac{v_d}{V}$ as a function of $\frac{r_c}{r_{min}}$ could not be found. In this section, we provide numerical simulations for specific cases. Figure 8 illustrates the obtained lower bound results (depicted in blue) using the following approach:

- For a predefined $\frac{r_c}{r_{min}}$, start with an initial guess for $\frac{v_d}{V}$ and run Algorithm 1 until the UAV has flown over the target position n times (in this case we have used $n = 4$). Stop if at any given path point, there is no solution for the desired path's angular velocity that complies with the UAV's kinematic constraints $\Rightarrow |\omega_{limit}| = []$ (cf. step 6 of Algorithm 1);
- Decrease the value of $\frac{v_d}{V}$ and repeat the previous step until the stop condition is achieved.

For the case where $\frac{r_c}{r_{min}} \geqslant 0.8$, these results are similar to the ones presented in [1] (used as a benchmark - depicted in red). For $\frac{r_c}{r_{min}} < 0.8$ it can be seen that the obtained lower bound gradually increases (with respect to the benchmark) as $\frac{r_c}{r_{min}}$ decreases. This is mainly related to the chosen desired path geometry and one can arguably infer that a better performance could be achieved if a more suited path was used. Moreover, note that the considered benchmark only applies to convoys moving with a specific constant heading and speed configuration (hence it corresponds to the optimal solution) while the computed lower bound for the proposed method always holds for the case of a convoy moving with constant heading and time-varying speed.

B. Convoy moving with relaxed restrictions

This section illustrates how the proposed method can be used to relax the convoy movements restrictions described in the literature, allowing it to have time-varying linear and angular velocities. In this simulation, the goal is to make the UAV to track a ground vehicle moving with time-varying linear and angular velocities by following a lemniscate path centered at the target position while computing the desired path's angular velocity ω_d using Algorithm 1 and the UAV yaw rate $\dot{\psi}$ using the MPF control law given by equation (7)

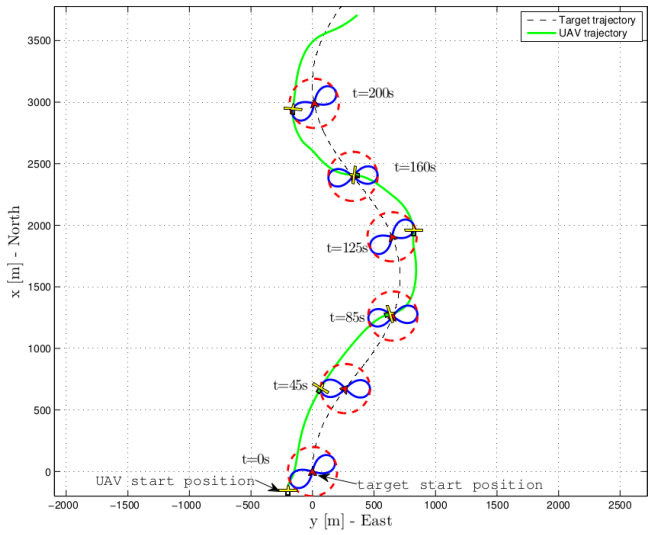

Fig. 9. UAV trajectory following a target with time-varying linear and angular velocities.

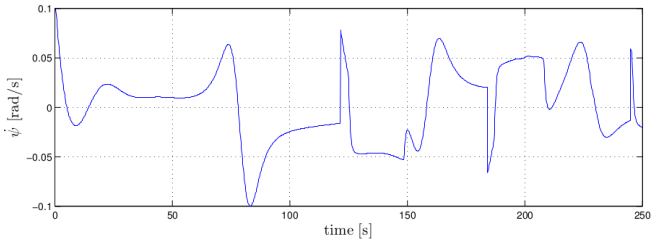

Fig. 10. Numerical simulation - UAV's angular velocity.

(see also [9]), to make the UAV converge to and track the desired moving path. The UAV speed is set to $V = 20$m/s, its minimum turning radius is set to $r_{min} = 200$m, and thus $\omega_{max} = 0.1$rad/s.

The target was moving according to

$$\begin{aligned}(p_{t_x},\ p_{t_y},\ \psi_t,\ \|v_t\|)|_{t=0} =&(0\text{m},\ 0\text{m},\ 0,\ 17\text{m/s})\\ \|\dot{v}_t\| =&0.01\sin(-0.07\,t)\ \text{m}/s^2\\ \dot{\psi}_t =&0.02\cos(0.03\,t)\ \text{rad}/s \end{aligned} \quad (11)$$

where v_t corresponds to the target velocity and ψ_t is the target heading. In order to attach the desired path to the target we set the path-transport frame with $p_0|_{t=0} = \left[\begin{array}{cc} p_{t_x} & p_{t_y}\end{array}\right]|_{t=0}$, $v_d = v_t$ and $\psi_d = \psi_t$. The MPF controller gains were set to $g_1 = 0.22$ and $g_2 = 0.0002$.

Figure 9 presents the obtained UAV's trajectory. The UAV, convoy center, convoy circle and desired moving path (depicted in blue) positions at sample time instants are also presented. The UAV always remains inside the convoy circle of interest (depicted in red) and its resulting trajectory (depicted in green) complies with its kinematic constraints (i.e., $|\dot{\psi}| < \omega_{max}$ - see Figure 10). The desired path angular velocity ω_d and orientation angle ψ_p obtained using Algorithm 1 are presented in Figure 11. The distance and angular errors (respectively y_F and $\tilde{\psi}$) of the UAV with respect to the desired moving path are depicted in Figure 12 showing the good performance of the control strategy.

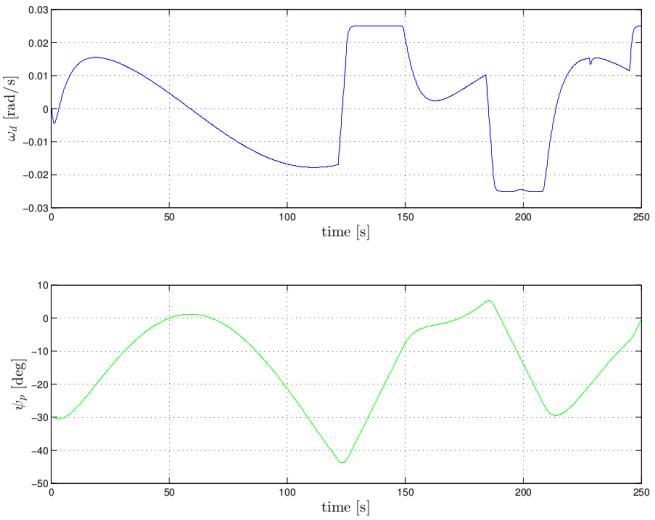

Fig. 11. Numerical simulation - desired path angular velocity ω_d and orientation angle ψ_p obtained using Algorithm 1.

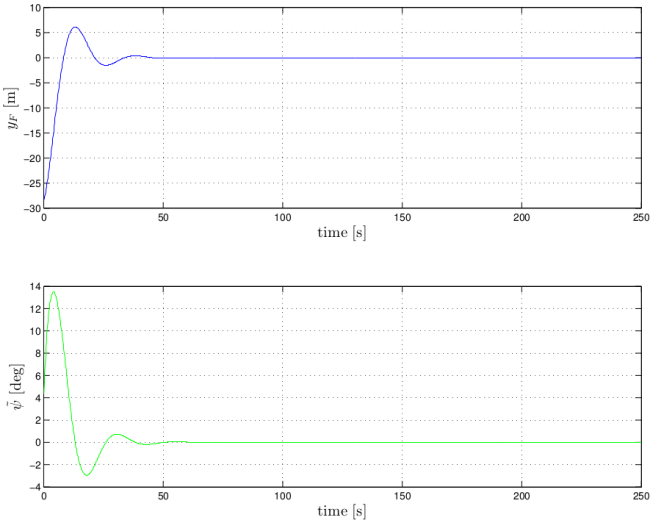

Fig. 12. Numerical simulation - position and heading errors.

C. Performance metric

The presented lower bound in Section V-A was computed by considering the case of a convoy moving with constant heading and speed. Despite we have demonstrated through a simulation example that the proposed method allows to relax the constraint on the convoy movements, a solution to obtain ω_{limit} that complies with the UAV kinematic restrictions (given by conditions (4) and (6)) for the general case of time-varying heading and speed of the convoy is not so straightforward to compute because it depends on the geometry of the problem and might not always exist. In that case, ω_{limit} is computed directly from condition (4) considering only the geometric constraints of the problem (see Step 7 of Algorithm 1). In order to ensure a favourable relative geometry (i.e., the relative orientation angle between the desired path and the convoy heading that allows the existence of solution for ω_{limit}) for the problem, it is

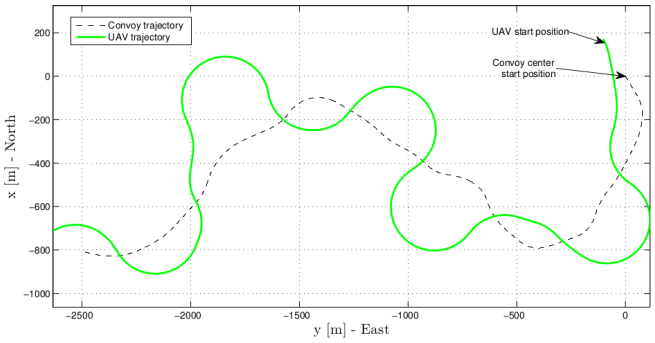

Fig. 13. Performance metric simulation - UAV and convoy center trajectories.

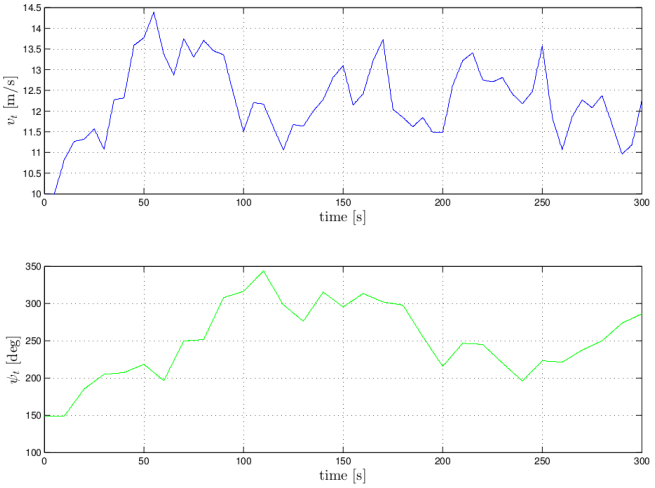

Fig. 14. Performance metric simulation - Convoy heading and speed.

desirable to have a small amplitude of the path orientation ψ_p with respect to the convoy velocity vector orientation ψ_d. Figure 4 provides a graphical illustration of this idea. This is implemented by Step 8 of Algorithm 1 where the path orientation angle ψ_p relative to the target heading ψ_d is contained within the interval $[-\frac{\pi}{6}, \quad \frac{\pi}{6}]$, using a proportional control law with $k_p = 0.3$.

Additionally, consider a scenario where the target/convoy kinematics does not always comply with the lower bound for the $\frac{v_d}{V}$ ratio computed in Section V-A, and thus, continuous convoy protection cannot be provided using a single UAV even in the case of a convoy moving with constant heading. Similarly to the strategy proposed in [1] one can consider a multi-UAV coordination approach together with a timing strategy to schedule the UAVs such that, at any time instant, one of the UAVs is inside the convoy circle. This, however, is out of the scope of this paper. Nevertheless, an interesting performance result in a realistic scenario where no bounds on the convoy movements are considered (except that $v_d < V$) is to compute the average time that a single fixed-wing UAV remains inside the convoy circle relative to the total simulation time, denoted by Av_t.

In order to compute the proposed performance metric we used 500 Monte Carlo simulations, where each simulation lasted 300 seconds. The target/convoy started moving with random heading ($\psi_t|_{t=0}$) according to a uniform distribution in the interval $]-\pi, \pi[$. The UAV's ground speed was chosen to be $V = 20$m/s and the UAV's minimum turning radius was set to $r_{min} = 200$m. In each simulation, the target/convoy center initial position $p_t|_{t=0s}$ was set at the origin of the inertial frame and the UAV initial position was set at a distance $d = r_{min}$ from the target/convoy center with the line of sight angle between the line that connects the target center of mass $p_t|_{t=0s}$ to the UAV center of mass $p_{t=0s}$ and North $\alpha_{LOS} = \psi_t|_{t=0} - \pi$. The UAV initial heading $\psi|_{t=0s}$ was set equal to the target/convoy initial heading $\psi|_{t=0s} = \psi_t|_{t=0}$. Both $\dot{v}_t$ and $\dot{\psi}_t$ were defined as stochastic signals with a normal distribution with a predefined mean and standard deviation, namely

$$\|\dot{v}_t\| \sim \mathcal{N}(0, 0.05)$$
$$\dot{\psi}_t \sim \mathcal{N}(0, 0.03)$$

with an output sample time set to 10s (simulation time). Two scenarios were considered for the proposed performance metrics. On the first one, the target's/convoy initial speed was set to $\|v_t\|_{t=0s} = 10$m/s and $\|v_t\|$ was limited to the interval $[0, \ 19]$ [m/s]. For the second scenario, the target's/convoy initial speed was set to $\|v_t\|_{t=0s} = 16$m/s and $\|v_t\|$ was limited to the interval $[15, \ 19]$ [m/s]. The speed bounds imposed on the second scenario took into account the lower bound for the v_d/V ratio presented in Section V-A, thus providing a more adequate performance metric for the proposed strategy. On both scenarios, the $\frac{r_c}{r_{min}}$ value was set equal to 1.

Figure 13 shows the obtained results for the convoy and UAV trajectories (for a particular simulation) using the above defined variables for the first scenario.

The corresponding convoy heading and speed are presented in Figure 14 illustrating the realistic scenario considered for the performance metric.

The performance metric was computed through

$$Av_t = \frac{1}{500} \sum_{i=1}^{500} \frac{t_{inside_i}(r_{c_i})}{300}$$

where r_{c_i} is the convoy circle radius at simulation i and t_{inside_i} is total time the UAV remains inside r_{c_i} during simulation i.

TABLE I
PROPOSED METHOD PERFORMANCE METRICS.

	Scenario 1	Scenario 2
Av_t	0.66	0.88

From the obtained results presented in Table I for the two considered scenarios, one can conclude that the proposed strategy provides a versatile solution for the convoy protection problem with unconstrained movements.

VI. Conclusions

MPF control laws allow a UAV to converge to and follow a path that is moving with respect to an inertial frame.

By setting the linear velocity of the reference path equal to the linear velocity of a convoy center, one can have a UAV following the convoy while the angular velocity of the reference path can be used to maximize the time that the convoy center remains within the UAV sensor footprint (assumed to be smaller than the UAV minimum turning radius) and make the resulting UAV trajectory comply with its kinematic constraints. The proposed method provides a versatile solution for the convoy protection problem with unconstrained movements.

The performance of the method depends on the geometry of the reference path and further work is necessary to study which is the best reference path to choose. Another open problem is the study of the robustness of the algorithm with respect to disturbances, namely strong winds. Future work also includes the experimental evaluation of the proposed method in real flight scenarios.

REFERENCES

[1] X. Ding, A. Rahmani, and M. Egerstedt, "Multi-UAV convoy protection: an optimal approach to path planning and coordination," *IEEE Transactions on Robotics*, vol. 26, pp. 256–268, 2010.

[2] O. Dobrokhodov, I. Kaminer, K. Jones, and R. Ghabcheloo, "Vision-based tracking and motion estimation for moving targets using small UAVs," in *Proceedings of the AIAA Guidance Navigation and Control Conference and Exibit*, 2006.

[3] E. Frew, D. Lawrence, C. Dixon, J. Elston, and J. Pisano, "Lyapunov guidance vector fields for unmanned aircraft applications," in *Proceedings of the 2007 American Control Conference*, 2007, pp. 371–376.

[4] H. Chen and K. Chang, "Tracking with UAV using tangent-plus-Lyapunov vector field guidance," in *Proceedings of the 12th International Conference on Information Fusion*, 2009.

[5] R. Anderson and D. Milutinovic, "Dubins vehicle tracking of a target with unpredictable trajectory," in *ASME 2011 Dynamic Systems and Control Conference and Bath/ASME Symposium on Fluid Power and Motion Control*, 2011, pp. 675–682.

[6] J. Lee, R. Huang, A. Vaughn, X. Xiao, K. Hedrick, M. Zennaro, and R. Sengupta, "Strategies of path-planning for a UAV to track a ground vehicle," in *Proceedings of the 2nd annual Autonomous Intelligent Networks and Systems Conference*, 2003.

[7] S. Spry, A. Girard, and K. Hedrick, "Convoy protection using multiple unmanned aerial vehicles: organization and coordination," in *Proceedings of the 2005 American Control Conference*, 2005.

[8] T. Oliveira, P. Encarnação, and A. Aguiar, "Moving path following for autonomous robotic vehicles," in *Proceedings of the European Control Conference (ECC)*, 2013.

[9] T. Oliveira, A. P. Aguiar, and P. Encarnação, "Moving path following for unmanned aerial vehicles with applications to single and multiple target tracking problems," *Conditionally accepted for publication on IEEE Transactions on Robotics*, 2016.

[10] L. Bishop, "There is more than one way to frame a curve," in *Amer. Math*. Monthly 82, March 1975, pp. 246–251.

[11] I. Kaminer, A. Pascoal, C. Cao, and V. Dobrokhodov, "Path following for unmanned aerial vehicles using L1 adaptive augmentation of commercial autopilots," *Journal of Guidance, Control and Dynamics*, vol. 33, pp. 550–564, 2010.

[12] L. Lapierre, D. Soetanto, and A. Pascoal, "Adaptive, non-singular path-following control of dynamic wheeled robots," in *Proceedings of the 42nd IEEE Conference on Decision and Control, vol. 2*, 2003, pp. 1765–1770.

[13] A. Rucco, A. Aguiar, and J. Hauser, "Trajectory optimization for constrained UAVs: a virtual target vehicle approach," in *Proceedings of the International Conference on Unmanned Aircraft Systems (ICUAS)*, 2015.

[14] E. W. Weisstein. (2016) Lemniscate. From MathWorld–A Wolfram Web Resource. [Online]. Available: http://mathworld.wolfram.com/Lemniscate.html